

A Rapid Hierarchical Rendering Technique for Translucent Materials

Henrik Wann Jensen
Stanford University

Juan Buhler
PDI/DreamWorks

Abstract

This paper introduces an efficient two-pass rendering technique for translucent materials. We decouple the computation of irradiance at the surface from the evaluation of scattering inside the material. This is done by splitting the evaluation into two passes, where the first pass consists of computing the irradiance at selected points on the surface. The second pass uses a rapid hierarchical integration technique to evaluate a diffusion approximation based on the irradiance samples. This approach is substantially faster than previous methods for rendering translucent materials, and it has the advantage that it integrates seamlessly with both scanline rendering and global illumination methods. We show several images and animations from our implementation that demonstrate that the approach is both fast and robust, making it suitable for rendering translucent materials in production.

Keywords: Subsurface scattering, BSSRDF, reflection models, light transport, diffusion theory, global illumination, realistic image synthesis

1 Introduction

Translucent materials are frequently encountered in the natural world. Examples include snow, plants, milk, cheese, meat, human skin, cloth, marble, and jade. The degree of translucency may vary, but the characteristic appearance is distinctly smooth and soft as a result of light scattering inside the objects, a process known as subsurface scattering. Subsurface scattering diffuses the scattered light and blurs the effect of small geometric details on the surface, softening the overall look. In addition, scattered light can pass through translucent objects; this is particularly noticeable when the objects are lit from behind. To render these phenomena and capture the true appearance of translucent materials it is therefore necessary to simulate subsurface scattering.

Traditionally subsurface scattering has been approximated as Lambertian diffuse reflection. This was later improved by Hanrahan and Krueger [1993] with an analytic term for single scattering in order to account for important directional effects. They also proposed a method for simulating subsurface scattering by tracing photons through the material, but in the end they used a BRDF (Bidirectional Reflectance Distribution Function [Nicodemus et al. 1977]) to represent the final model. A BRDF only accounts for scattering at a single point, and it cannot be used to simulate light transport

within the material between different points on the surface. This requires treating the material as a participating medium with a surface. This was done by Dorsey et al. [1999] who used photon mapping to simulate subsurface scattering in weathered stone. Pharr and Hanrahan [2000] introduced the concept of scattering equations and demonstrated how this concept could be used to simulate subsurface scattering more efficiently than traditional Monte Carlo ray tracing.

More recently, Koenderink and van Doorn [2001] and Jensen et al. [2001] proposed modeling the scattering of light in translucent materials as a diffusion process. The diffusion approximation works particularly well in highly scattering media where traditional Monte Carlo ray tracing becomes very expensive [Stam 1995]. Jensen et al. [2001] suggested a simple analytical dipole diffusion approximation and found this model to be in good agreement with measurements of light scattered from translucent materials. They used this approximation to formulate a complete BSSRDF (Bidirectional Scattering Surface Reflectance Distribution Function [Nicodemus et al. 1977]), which relates outgoing radiance at a point to incident flux at all points on the surface. Finally, they evaluate the BSSRDF by sampling the incident flux on the surface.

The BSSRDF approximation [Jensen et al. 2001] is much faster than Monte Carlo photon tracing. However, since it requires sampling the incident flux distribution at the surface, it is still more expensive to evaluate than a traditional BRDF. It is particularly expensive for highly translucent materials where light can scatter a long distance within the material. Another difficulty with the approach is that it only includes internal scattering in the material due to direct illumination from the light sources. It is not obvious how to extend the sampling technique to include global illumination as well.

In this paper we introduce a fast and general two-pass rendering technique for translucent materials. Our approach is based on two key ideas. The first idea is to decouple of the computation of the incident illumination from the evaluation of the BSSRDF by using a two-pass approach. In the first pass, we compute the irradiance at selected points on the surface, and in the second pass we evaluate a diffusion approximation using the pre-computed irradiance samples. The second idea is to use a rapid hierarchical evaluation of the diffusion approximation using the pre-computed irradiance samples. This approach is substantially faster than directly sampling the BSSRDF since it only evaluates the incident illumination once at a given surface location, and it is particularly efficient for highly translucent materials where sampling the BSSRDF is costly. To evaluate the irradiance, we can use standard rendering techniques including scanline rendering and global illumination methods. This means that we can compute the effects of indirect illumination on translucent materials. Furthermore, our results do not suffer from any high-frequency Monte Carlo sampling noise since the hierarchical evaluation is deterministic. This is a great advantage for animations where this type of noise is particularly noticeable.

Another contribution of this paper is a reformulation of the scattering parameters for translucent materials. We show how the intrinsic scattering properties of translucent materials can be computed from two intuitive parameters: a diffuse reflectance and an average scattering distance. Finally, we show several results from our implementation of the method in a scanline renderer as well as

a Monte Carlo ray tracer. Our results indicate that the hierarchical evaluation technique is fast and robust, and capable of rendering images and animations of translucent objects in complex lighting environments.

2 Light Diffusion in Translucent Materials

The scattering of light within a medium is described by the radiative transport equation [Chandrasekhar 1960]:

$$(\vec{\omega} \cdot \nabla)L(x, \vec{\omega}) = -\sigma_t L(x, \vec{\omega}) + \sigma_s L_i(x, \vec{\omega}) + s(x, \vec{\omega}). \quad (1)$$

Here, L is the radiance, s is a source term, σ_s is the scattering coefficient, σ_a is the absorption coefficient, σ_t is defined as $\sigma_a + \sigma_s$, and L_i is the in-scattered radiance:

$$L_i(x, \vec{\omega}) = \int_{4\pi} p(\vec{\omega}, \vec{\omega}') L(x, \vec{\omega}') d\vec{\omega}'. \quad (2)$$

The phase function, p , specifies the spherical distribution of the scattered light. It is normalized, $\int_{4\pi} p(\vec{\omega}, \vec{\omega}') d\vec{\omega}' = 1$, and we assume it only depends on the cosine of the scattering angle, $p(\vec{\omega}, \vec{\omega}') = p(\vec{\omega} \cdot \vec{\omega}')$. The mean cosine, g , of the scattering angle is:

$$g = \int_{4\pi} p(\vec{\omega}, \vec{\omega}') (\vec{\omega} \cdot \vec{\omega}') d\vec{\omega}'. \quad (3)$$

The value of $g \in [-1, 1]$ indicates the type of scattering in the medium. $g = 0$ is isotropic scattering, $g < 0$ is backwards scattering and $g > 0$ is forward scattering. Most translucent materials are strongly forward scattering with $g > 0.7$ (skin for example has $0.7 < g < 0.9$ [Gemert et al. 1989]). Such strongly peaked phase functions are costly to simulate in media with multiple scattering since the probability of sampling in the direction of the light sources will be low in most situations. The difficulty of sampling further increases with the distance to the light sources. In this case we can benefit from a powerful technique known as the *similarity of moments* [Wyman et al. 1980], which allows us to change the scattering properties of the medium without significantly influencing the actual distribution of light. Specifically, we can modify the medium to have isotropic scattering ($g = 0$) by changing the scattering coefficient to

$$\sigma'_s = (1 - g)\sigma_s, \quad (4)$$

where σ'_s is the *reduced* scattering coefficient. The absorption coefficient remains unchanged, and we get the reduced extinction coefficient $\sigma'_t = \sigma'_s + \sigma_a$.

Equation 1 is a five-dimensional integro-differential equation, and even in media with isotropic scattering it is in most cases difficult to solve. One approach is to expand radiance into a truncated series of spherical harmonics. For this purpose we divide the radiance into two components: the unscattered radiance, L_u , and the scattered (diffuse) radiance, L_d . The unscattered radiance is reduced as a function of the distance traveled through the medium [Ishimaru 1978]:

$$L_u(x + \Delta x, \vec{\omega}) = e^{-\sigma'_t \Delta x} L_u(x, \vec{\omega}). \quad (5)$$

The average distance at which the light is scattered, the mean-free path, is $\ell_u = 1/\sigma'_t$.

The diffusion approximation uses the first four terms of the spherical harmonic expansion to represent L_d :

$$L_d(x, \vec{\omega}) \approx F_t(x) + \frac{3}{4}\pi \vec{E}(x) \cdot \vec{\omega}. \quad (6)$$

The 0th-order spherical harmonic, the radiant fluence, F_t , is $F_t(x) = \int_{4\pi} L_d(x, \vec{\omega}') d\vec{\omega}'$, and the 3 terms of the 1st-order spherical harmonic, the vector irradiance, \vec{E} , is $\vec{E} = \int_{4\pi} L_d(x, \vec{\omega}') \vec{\omega}' d\vec{\omega}'$. Note that L_d cannot be purely diffuse as this would result in zero flux within the medium. Instead L_d is approximated as being mostly diffuse, but with a preferential direction (as indicated by \vec{E}) to the overall flow of the flux.

The diffusion approximation is particularly effective in highly scattering media at some distance from the light sources as well as in regions with rapidly changing scattering properties. This is due to the natural smoothing resulting from multiple scattering [Stam 1995]. More precisely, the diffusion approximation has been shown [Furutsu 1980] to be accurate when $\sigma_a/\sigma_t \ll 1 - g^2$.

Applying the diffusion approximation (Equation 6) to the radiative transport equation (Equation 1) yields the diffusion equation (the details of the derivation can be found in [Ishimaru 1978]):

$$\frac{1}{3\sigma'_t} \nabla^2 F_t(x) = \sigma_a F_t(x) - S_0(x) + \frac{1}{\sigma'_t} \nabla \cdot \vec{S}_1(x). \quad (7)$$

Here, S_0 and S_1 represents the 0th- and the 1st-order spherical harmonics expansion of the source term, similar to the expansion for diffuse radiance.

The diffusion equation can be solved analytically for special cases [Ishimaru 1978], or by using a multigrid approach [Stam 1995]. In the case of translucent materials, we are interested in the outgoing radiance at the material surface as a function of the incoming radiance. Jensen et al. [2001] use a dipole diffusion approximation for a point source in a semi-infinite medium. The point source is an approximation of an incoming beam of light for which it is assumed that all light scatters at a depth of one mean-free path below the surface. The dipole diffusion approximation results in the following expression for the radiant exitance, M_o , at surface location x_o due to incident flux, $\Phi_i(x_i)$, at x_i :

$$dM_o(x_o) = d\Phi_i(x_i) \frac{\alpha'}{4\pi} \left\{ C_1 \frac{e^{-\sigma_{tr} d_r}}{d_r^2} + C_2 \frac{e^{-\sigma_{tr} d_v}}{d_v^2} \right\}, \quad (8)$$

where

$$C_1 = z_r \left(\sigma_{tr} + \frac{1}{d_r} \right) \quad \text{and} \quad C_2 = z_v \left(\sigma_{tr} + \frac{1}{d_v} \right). \quad (9)$$

Here, $\alpha' = \sigma'_s/\sigma'_t$ is the reduced albedo, $\sigma_{tr} = \sqrt{3\sigma_a\sigma'_t}$ is the effective transport extinction coefficient, $d_r = \sqrt{r^2 + z_r^2}$ is the distance to the real light source, $d_v = \sqrt{r^2 + z_v^2}$ is the distance to the virtual source, $r = \|x_o - x_i\|$ is the distance from x_o to the point of illumination, and $z_r = \ell_u$ and $z_v = \ell_u(1 + 4/3A)$ are the distance from the the dipole lights to the surface (shown in Figure 2). Finally, the boundary condition for mismatched interfaces is taken into account by the A term which is computed as $A = (1 + F_{dr})/(1 - F_{dr})$, where the diffuse Fresnel term, F_{dr} is approximated from the relative index of refraction η by [Groenhuis et al. 1983]:

$$F_{dr} = -\frac{1.440}{\eta^2} + \frac{0.710}{\eta} + 0.668 + 0.0636\eta. \quad (10)$$

In addition to Equation 8 the BSSRDF includes a single scattering term (see [Jensen et al. 2001] for the details).

2.1 The Importance of Multiple Scattering

The diffuse term is the most costly to sample for translucent materials since it depends on lighting from a large fraction of the material surface. We can approximate the average distance, $\ell_d = 1/\sigma_{tr}$,

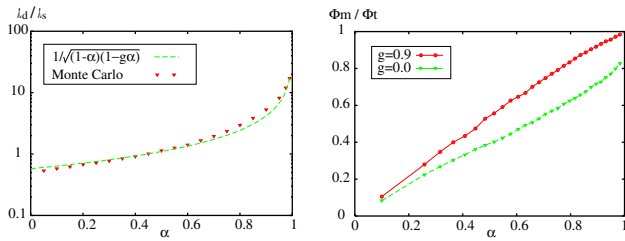


Figure 1: These graphs show the effect of increasing the scattering albedo of the material. The left graph shows the average scattering distance for diffuse radiance divided by the mean-free path for single scattering (for $g = 0.9$) as predicted by Equation 11 and estimated using a Monte Carlo photon simulation. The graph on the right shows the fraction of the radiant exitance that is due to multiple scattering (estimated with a Monte Carlo photon simulation). The important thing to notice in the two graphs is that the diffuse radiance scatters much further, and that it becomes increasingly important as the albedo gets closer to one.

along the surface that the diffused radiance scatters by assuming that the exponential term dominates in Equation 8. By dividing this distance with the mean-free path, $\ell_s = 1/\sigma_t$, of single-scattered light, we can estimate the relative scattered distance of the two within the medium:

$$\frac{\ell_d}{\ell_s} = \frac{\sigma_t}{\sigma_{tr}} = \frac{1}{\sqrt{3(1-\alpha)(1-g\alpha)}}. \quad (11)$$

Note how the ratio depends only on the albedo, α , and the scattering anisotropy, g . Figure 1 shows a plot of this equation and a comparison with a Monte Carlo photon simulation. For the photon simulation, we traced photons from random directions towards a translucent material and recorded the average distance at which the photons left the surface again after scattering inside the material. This distance divided by ℓ_s is shown in the graph. For the simulation we used the Henyey-Greenstein phase function [Henyey and Greenstein 1941] and the photons are scattered using the approach described by Hanrahan and Krueger [1993]. Despite several assumptions about the average scattering distance, it can be seen that the predictions of Equation 11 are surprisingly accurate. For both simulations the ratio rapidly increases as the albedo approaches one as a consequence of the increasing number of scattering events. From the measurements in [Jensen et al. 2001] we can see that all of the materials have an albedo close to one. As an example, red wavelengths in skim milk (assuming $g = 0.9$) have a scattering albedo of $\alpha \approx 0.9998$, which gives a ratio $\ell_d/\ell_s \approx 129$. This means that the average distance traveled by diffuse radiance is 129 times larger than the average distance traveled by unscattered radiance. In effect this means that single scattering is substantially more localized than diffuse scattering.

The importance of multiple scattering increases with the albedo of the material. To further investigate how important multiple scattered light is for translucent materials, we performed another Monte Carlo photon simulation. In this simulation we traced photons from random directions towards the surface scattering medium. At the surface we recorded the radiant exitance from the photons that scattered in the medium. We used an index of refraction of 1.3 for the medium (the results are very similar for other values). Two important parameters for the medium are the scattering anisotropy and the scattering albedo. The right graph in Figure 1 shows the fraction of the radiant exitance from the material due to multiple scattered light as a function of the albedo. Note, how the fraction gets close to 1.0 for the forward scattering material, and close to 0.9 for a material with isotropic scattering.

3 A Two-Pass Technique for Evaluating the Diffusion Approximation

As shown in the previous section, the radiant exitance from highly scattering translucent materials is dominated by photons that have scattered multiple times inside the material. Jensen et al. [2001] compute the contribution from multiple scattering by sampling the irradiance at the material surface and evaluating the diffusion approximation — in effect convolving the reflectance profile predicted by the diffusion approximation with the incident illumination. Even though the diffusion approximation is a very effective way of approximating multiple scattering, this sampling technique becomes expensive for highly translucent materials. The reason for this is that the sampled surface area grows and needs more samples as the material becomes more translucent.

The key idea for making this process faster is to decouple the computation of irradiance from the evaluation of the diffusion approximation. This makes it possible to reuse irradiance samples for different evaluations of the diffusion equation. For this purpose, we use a two-pass approach in which the first pass consists of computing the irradiance at selected points on the surface, and the second pass is evaluating the diffusion approximation using the precomputed irradiance values. For the second pass we exploit the decreasing importance of distant samples and use a rapid hierarchical integration technique.

Pass 1: Sampling the Irradiance

To obtain the sample locations on the surface of a piece of geometry we use Turk’s point repulsion algorithm [Turk 1992], which produces a uniform sampling of points on a polygon mesh. We do not change (retille) our mesh as we only need the point locations. To ensure an accurate evaluation of the diffusion approximation we need enough points to account for several factors including the geometry, the variation in the lighting, the scattering properties of the material, and the integration technique. We use the mean-free path, ℓ_u , as the maximum distance between the points on the surface. The approximate number of points that we use for a given object then becomes $A/(\pi\ell_u^2)$, where A is the surface area of the object. This is a conservative estimate, since anything below the mean-free path will be blurred by multiple scattering. However, the sample density should not be much lower since this will result in low-frequency noise in the reconstruction of the diffusion approximation. Note that our reconstruction does not require a uniform sampling since we weight each sample point by the area associated with the point. It would be possible to use other approaches that sample more densely around discontinuities in the irradiance or the geometry.

With each sample point we store the location, the area associated with the point (in the case of uniform sampling, this is simply the surface area divided by the number of points), and a computed irradiance estimate. Since the irradiance is computed at a surface location we can use standard rendering techniques including methods that account for global illumination (such as photon mapping [Jensen 1996] and irradiance caching [Ward et al. 1988]).

Pass 2: Evaluating the Diffusion Approximation

The diffusion approximation can be evaluated directly (using Equation 8) by summing the contribution from all the irradiance samples. However, this approach is costly since most objects have several thousand irradiance samples. Another, strategy would be to only consider nearby “important” points. This approach would work, but it could potentially leave out important illumination, and for accurate evaluations it would still need hundreds of irradiance samples (e.g. our sampling produces roughly 300 samples within a disc with a radius of 10 mean-free paths). Instead we use a hierarchical evaluation technique which takes into account the contribution

from all irradiance samples by clustering distant samples to make this evaluation fast. The exponential shaped fall-off in the diffusion approximation makes the hierarchical approach very efficient. The concept is similar to the hierarchical approaches used for N-body problems [Appel 1985].

Several different hierarchical structures can be used for the irradiance samples. We use an octree in our implementation. Each node in the tree stores a representation of illumination in all its child nodes: the total irradiance, E_v , the total area represented by the points, A_v , and the average location (weighted by the irradiance) of the points, \bar{P}_v . To increase efficiency we allow up to 8 irradiance samples in a leaf voxel.

The total radiant exitance flux at a location, x , is computed by traversing the octree from the root. For each voxel we check if it is “small enough” or if it is a leaf node that it can be used directly; otherwise all the child nodes of the voxel are evaluated recursively. If the point x is inside the voxel then we always evaluate the child nodes. For all other voxels we need an error criterion that specifies the desired accuracy of the hierarchical evaluation. One option would be to compute the potential contribution from the voxel and decide based on this estimate if the voxel should be subdivided. Unfortunately, this is not trivial — and simply using the center of the points in the voxel is not a good approximation for nearby large voxels. Instead we use a much simpler criterion that is both fast to evaluate and that works well in practice. We base our criteria for subdividing a voxel on an approximation of the maximum solid angle, $\Delta\omega$, spanned by the points in the voxel:

$$\Delta\omega = \frac{A_v}{\|\bar{x} - \bar{P}_v\|^2}. \quad (12)$$

To decide if a voxel should be subdivided we simply compare $\Delta\omega$ to a value ϵ which controls the error. If $\Delta\omega$ is larger than ϵ then the children of the voxel are evaluated; otherwise the voxel is used directly. Another option would be to check the solid angle of the voxel itself; however, using the area of the points makes the evaluation faster, since we can use the clustered values for large voxels with just a few irradiance samples (e.g. large voxels that just barely intersect the surface).

The radiant exitance due to a voxel is evaluated using the clustered values for the voxel, or if it is a leaf-voxel by summing the contribution from each of the points in the voxel. The radiant exitance, $M_{o,p}(x)$ at x from a given irradiance sample is computed using the dipole diffusion approximation

$$M_{o,p}(x) = F_{dt}(x) \frac{dM_o(x)}{\alpha' d\Phi_i(\bar{P}_p)} E_p A_p, \quad (13)$$

where P_p is the location of the irradiance sample(s), E_p is the irradiance at that location, and A_p is the area of the location. $dM_o(\|x - \bar{P}_p\|_2)/(\alpha' d\Phi_i(\bar{P}_p))$ is computed using Equation 8. Notice that we scale each irradiance sample by the diffuse Fresnel transmittance, $F_{dt} = 1 - F_{dr}$ (F_{dr} is computed using Equation 10). This is necessary when approximating the irradiance by the dipole source. We could have scaled the contribution from each of the sample rays used to compute the irradiance by the true Fresnel transmittance, but by using the diffuse (Lambertian) assumption we can benefit from fast rendering techniques for diffuse materials (e.g. caching techniques such as photon maps [Jensen 1996] and irradiance caching [Ward et al. 1988]). The dipole approximation for an irradiance sample is illustrated in Figure 2. Note that this approximation has been derived assuming a semi-infinite medium. In the presence of complex geometry (e.g. curved surfaces or thin geometry) we use the same techniques as Jensen et al. [2001] to ensure numerical stability.

The result of traversing and evaluating the voxels is an estimate of the total (diffuse) radiant exitance, M_o at x , which we convert into radiance, L_o :

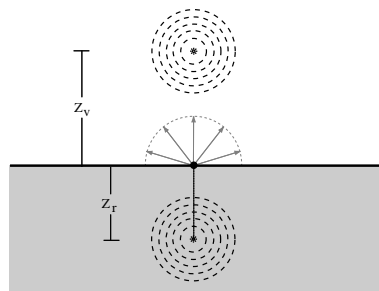


Figure 2: For each point sample we use the dipole diffusion approximation to compute the radiant exitance.

$$L_o(x, \vec{\omega}) = \frac{F_t(x, \vec{\omega})}{F_{dr}(x)} \frac{M_o(x)}{\pi}. \quad (14)$$

We scale the contribution by the Fresnel transmittance, F_t to account for reflection and transmission at the surface. Since, the diffusion approximation already includes a diffuse Fresnel transmittance we divide by F_{dr} . Alternatively, we could omit the Fresnel terms and assume a diffuse radiance.

4 Reparameterizing the BSSRDF

One difficulty in simulating subsurface scattering is that it is difficult to predict the resulting appearance from a given combination of absorption and scattering coefficients (since their effect is highly non-linear). In this section, we will outline a simple technique for reparameterizing the BSSRDF into using intuitive translucency and reflectivity parameters. These parameters are already present in the computations in the form of the diffuse mean free path ℓ_d and the diffuse reflectance of the material, and they are sufficient for computing the scattering and absorption properties of the material.

First, using the diffuse reflection coefficient (see [Jensen et al. 2001]), we solve for the reduced albedo of the material:

$$R_d = \frac{\alpha'}{2} \left(1 + e^{-\frac{4}{3}A\sqrt{3(1-\alpha')}} \right) e^{-\sqrt{3(1-\alpha')}}. \quad (15)$$

This equation is not easily invertible, but it has a simple monotonic shape in the valid region $\alpha' \in [0 : 1]$, and we use a few iterations of a simple secant root finder to compute α' .

We know the effective transport coefficient, $\sigma_{tr} \approx 1/\ell_d$, and given the reduced albedo we can find the reduced extinction coefficient:

$$\frac{\sigma_{tr}}{\sigma'_t} = \sqrt{3(1-\alpha')} \longrightarrow \sigma'_t = \frac{\sigma_{tr}}{\sqrt{3(1-\alpha')}} \quad (16)$$

Finally, this gives us the absorption and the reduced scattering coefficients: $\sigma'_s = \alpha' \sigma'_t$ and $\sigma_a = \sigma'_t - \sigma'_s$. If the scattering anisotropy, g , is given then the real extinction and scattering coefficients can be computed as well.

5 Results

In this section we present several results from our implementation of the rendering technique. We have used two different systems to implement the model: A Monte Carlo ray tracer with support for global illumination, and a modified a-buffer renderer used in production. Our timings were recorded on a dual 800MHz Pentium 3 for images with a width of 1024 pixels and 4 samples per pixel.

The first example include several renderings of a translucent marble teapot as shown in Figure 3. All of these images were rendered with the Monte Carlo ray tracer. The left column shows a comparison with the BSSRDF sampling technique by Jensen et

al. [2001], and our hierarchical technique under the same lighting conditions (for this comparison we use the BRDF approximation for the single scattering term). The important thing to notice is that the two images are practically indistinguishable except for a small amount of sampling noise in the BSSRDF image. This shows that the hierarchical approach is capable of matching the output of the BSSRDF for a translucent material. However, the hierarchical technique took just 7 seconds to render (including 1 second to compute the irradiance values at the samples), while the BSSRDF sampling took 18 minutes — a factor of 154 speedup in this case. The speedup will be even more dramatic for objects that are more translucent. The top image in the right column shows a glossy teapot illuminated by a high dynamic range environment map [Debevec 1999]. To enhance the translucency effect we made the environment black behind the camera. The render time for the image without glossy reflection is 7 seconds (the rendering time including glossy reflection is 40 seconds). The precomputation time for the irradiance samples (sampling the environment map) was roughly 1 minute. This scene would be extremely costly to render using the BSSRDF sampling approach, since it would involve picking a point on the light source and then sampling in the direction of the teapot — a process where the probability of generating good samples is very low. Finally, the lower right image shows the 150,000 sample locations on the teapot that we used for all images.

Our second example in Figure 4 shows the classic Cornell box global illumination scene with a translucent box. This image was rendered using Monte Carlo ray tracing — we used photon mapping [Jensen 1996] to speed up the computation of global illumination. Note the light scattering through the box, and the color bleeding in the scene. In the precomputation of the indirect illumination for the irradiance samples on the translucent box we used a diffuse assumption in order to account for multiple reflections between the box and the walls. However we do account for translucency when evaluating color bleeding on the wall. For scenes where translucency is important for the indirect illumination of the translucent elements (e.g. light bleeding through a leaf onto a white floor which then reflects back on the leaf) a multi-pass approach could be used where the indirect illumination is computed recursively for the translucent materials. The rendering time for the image was 55 seconds, and the precomputation of the irradiance for 20,000 points on the box was 21 seconds.

Our third example in Figure 6 shows the lower half of a face model rendered using a standard skin shader (on the left) and using a skin shader with support for translucency (on the right). This face model was built before the translucency shader was developed. It uses several textures, which we apply by scaling the 250,000 irradiance samples with filtered texture values (the filter support is equal to the area associated with each irradiance sample). This approach made it possible to replace the previous skin shader with a translucent version. The added translucency vastly increases the realism of the model as it softens the appearance of the skin and naturally simulates effects such as the color bleeding around the nose. The rendering time using the standard skin shader was 16 minutes while the translucent skin shader took 20 minutes (including generating the sample points). A significant advantage of our approach is that it works with all the standard lights used in production such as fill lights, rim lights and key lights. This natural integration of the translucency shader in the production framework made it a natural choice for the main character in “Sprout” (a short animation). Translucency helps depict the small size of the character as shown in Figure 5.

6 Conclusion and Future Work

We have presented an efficient two-pass rendering technique for translucent materials. We combine a point sampling of the irradi-

ance on the surface with a fast hierarchical evaluation of a diffusion approximation. Our approach is particularly efficient for highly translucent materials where the BSSRDF sampling [Jensen et al. 2001] becomes costly, and it integrates seamlessly with both scan-line rendering and global illumination methods. Our results demonstrate how the technique is both fast and robust making it suitable for rendering translucent materials in production of computer animations.

Future improvements include extending the approach to translucent materials with a visible internal 3D structure. It would also be useful to investigate the accuracy of the dipole diffusion approximation in the presence of complex geometry.

Another interesting path to explore is interactive rendering of translucent materials. This could be done by further simplifying the evaluation technique so that it can be implemented directly on programmable graphics hardware.

7 Acknowledgments

Thanks to the SIGGRAPH reviewers and to Maryann Simmons, Mike Cammarano, Pat Hanrahan, and Marc Levoy for helpful comments. The first author was supported by NSF ITR (IIS-0085864). The second author was supported by PDI/DreamWorks and by the PDI R&D group and thanks them for supporting the development and publication of these techniques.

References

- APPEL, A. 1985. An efficient program for many-body simulations. *SIAM Journal of Scientific Statistical Computing* 6, 85–103.
- CHANDRASEKHAR, S. 1960. *Radiative Transfer*. Oxford Univ. Press.
- DEBEVEC, P., 1999. St. Peter’s Basilica (www.debevec.org/probes/).
- DORSEY, J., EDELMAN, A., JENSEN, H. W., LEGAKIS, J., AND PEDERSEN, H. K. 1999. Modeling and rendering of weathered stone. In *Proceedings of SIGGRAPH’99*, 225–234.
- FURUTSO, K. 1980. Diffusion equation derived from space-time transport equation. *J. Opt. Soc. Am* 70, 360.
- GEMERT, M., JACQUES, S., STERENBORG, H., AND STAR, W. 1989. Skin optics. *IEEE Trans. on Biomedical Eng.* 16, 1146–1156.
- GROENHUIS, R. A., FERWERDA, H. A., AND BOSCH, J. J. T. 1983. Scattering and absorption of turbid materials determined from reflection measurements. I: Theory. *Applied Optics* 22, 2456–2462.
- HANRAHAN, P., AND KRUEGER, W. 1993. Reflection from layered surfaces due to subsurface scattering. In *Computer Graphics (SIGGRAPH’93 Proceedings)*, 165–174.
- HENYEV, L., AND GREENSTEIN, J. 1941. Diffuse radiation in the galaxy. *Astrophysics Journal* 93, 70–83.
- ISHIMARU, A. 1978. *Wave Propagation and Scattering in Random Media*, vol. 1. Academic Press, New York.
- JENSEN, H. W., MARSCHNER, S. R., LEVOY, M., AND HANRAHAN, P. 2001. A practical model for subsurface light transport. In *Proceedings of SIGGRAPH 2001*, 511–518.
- JENSEN, H. W. 1996. Global illumination using photon maps. In *Rendering Techniques ’96*, Springer Wien, X. Pueyo and P. Schröder, Eds., 21–30.
- KOENDERINK, J., AND VAN DOORN, A. 2001. Shading in the case of translucent objects. In *Proceedings of SPIE*, vol. 4299, 312–320.
- NICODEMUS, F. E., RICHMOND, J. C., HSIA, J. J., GINSBERG, I. W., AND LIMPERRIS, T. 1977. Geometric considerations and nomenclature for reflectance. Monograph 161, National Bureau of Standards (US), Oct.
- PHARR, M., AND HANRAHAN, P. 2000. Monte carlo evaluation of non-linear scattering equations for subsurface reflection. In *Proceedings of SIGGRAPH 2000*, 75–84.
- STAM, J. 1995. Multiple scattering as a diffusion process. In *Eurographics Rendering Workshop 1995*, Eurographics.
- TURK, G. 1992. Re-tiling polygonal surfaces. In *Computer Graphics (SIGGRAPH ’92 Proceedings)*, vol. 26, 55–64.
- WARD, G. J., RUBINSTEIN, F. M., AND CLEAR, R. D. 1988. A ray tracing solution for diffuse interreflection. In *Computer Graphics (SIGGRAPH ’88 Proceedings)*, vol. 22, 85–92.
- WYMAN, D. R., PATTERSON, M. S., AND WILSON, B. C. 1980. Similarity relations for anisotropic scattering in monte carlo simulations of deeply penetrating neutral particles. *J. Comp. Physics* 81, 137–150.



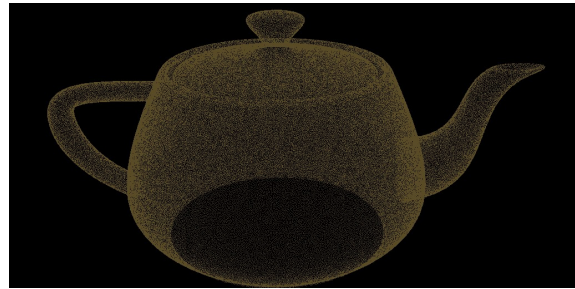
BSSRDF: sampled evaluation - 18 minutes



Illumination from a HDR environment



BSSRDF: hierarchical evaluation - 7 seconds



The sample locations on the teapot

Figure 3: A translucent teapot. On the left we compare our hierarchical BSSRDF evaluation (bottom) to a sampled BSSRDF (top). The top right image shows the teapot in a HDR environment, and the bottom right shows the 150,000 sample points on the teapot.

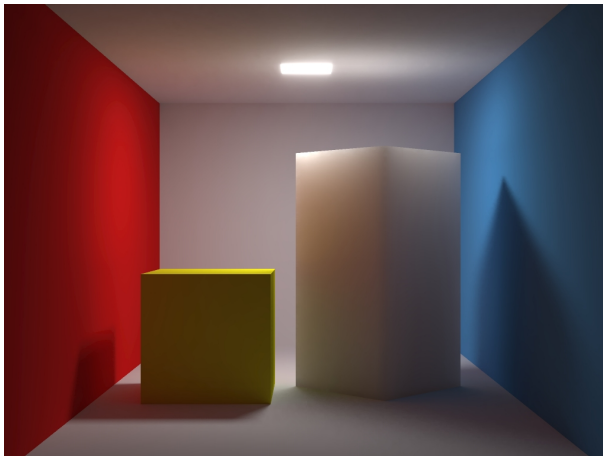


Figure 4: A global illumination scene with a translucent box. Note the light bleeding through the box, and the color bleeding in the model.



Figure 5: An animation with a translucent character. Translucency helps depict the small size of the character. Image courtesy of Scott Peterson - PDI/DreamWorks.



Figure 6: A textured face model lit by three light sources (key, fill, and rim). The left image shows the result using the skin shader that was used in the movie "Shrek", and the right image shows the result after adding our simulation of translucency to this shader.